Research Signpost
37/661 (2), Fort P.O., Trivandrum-695 023, Kerala, India

The Nanomechanics in Italy, 2007: 75-107 ISBN: 978-81-308-0237-4
Editor: Nicola Maria Pugno

5 Atomistic approach to nanomechanics: Concepts, methods, and (some) applications

Pierluca Palla, Mariella Ippolito, Stefano Giordano
Alessandro Mattoni and Luciano Colombo
Department of Physics, University of Cagliari and SLACS (CNR-INFM)
Cittadella Universitaria, I-09042 Monserrato (Ca), Italy

Abstract

In this work we describe the main concepts and the theoretical methods (rather than their numerical implementation) underlying the atomic-scale modelling of the mechanical properties (mainly, fracture-related features) in convalently bonded materials. Focus is given on the generation of interatomic potentials, which could result to be quantitatively reliable in describing the mechanical behaviour of complex

Correspondence/Reprint request: Prof. Luciano Colombo, Department of Physics – University of Cagliari Cittadella Universitaria, I-09042 Monserrato (Ca), Italy. E-mail: luciano.colombo@dsf.unica.it

(i.e. nano-structured) systems. In particular, we establish a conceptual guideline for the development of atomic force models, as based on a direct link between continuum and discrete solid mechanics. Furthermore, we describe a procedure aimed at generating interatomic potentials, properly accounting for brittle bonding in group-IV materials. Finally, we review a recent application of atomistic simulations to the investigation of the failure strength in silicon carbide containing nanovoids.

This work is based on the research effort ongoing at the Department of Physics of the University of Cagliari. For more details and a full list of published articles, please visit the Web site: http://www.dsf.unica.it/ colombo .

1. Introduction

By tradition, continuum mechanics has been used to model the macroscopic mechanical behavior of solid bodies (like, e.g., elastic or plastic deformations, failure strength, fracture mechanics) while quantum mechanics has been used at the nanoscale, where electronic features dominate. More recently, however, it has been widely recognized that, although specific approaches exist to tackle a problem at a given observation scale, different methodologies must be concurrently integrated in order to properly modeling the interplay between phenomena occurring at different length scales. This idea leads to the multiscale modeling approach: a paradigm effectively coupling different methods so as to provide a unique theoretical device able to pass physical information across different scales [1]. Typically, the mechanical properties can be described by combining macroscopic continuum homogenization theories with atomistic simulations. These latter provide the nanoscale complex behavior of the system at the most fundamental level, i.e. at the level of the collective response of an interacting assembly of atoms [2].

Concurrency of different methods is a very promising perspective currently under extensive investigation, but it is important to stress that in any case the atomic scale represents the smallest length scale at which such a multiscale paradigm must operate. Therefore, a robust and reliable model of atomic interactions - properly accounting for nanostructure evolution - is mostly needed. Such a model can be developed at different levels of erudition, the most fundamental one being quantum mechanical. The best reliable and transferable quantum approach available at present is the first principle (ab initio) molecular dynamics method, based on the density functional theory and implemented by the renowned Car-Parrinello method [3]. Here the only input requested to proceed is the atomic number of the chemical species present in the simulated system. Unfortunately, the numerical implementation of the Car-Parrinello scheme is quite demanding

in terms of computational workload and, even with the ever-increasing power of modern digital computers and the devolpement of novel linear scaling algorithms, its practical applications are still limited to systems containing no more than few hundreds of particles. This is good enough for coping with a lot of fundamental materials problems, but it leaves many others relevant to their mechanical response simply out of reach.

Alternatively, one can develop interatomic force models based on empirical potentials. In this case, any ambition of ab initio description is lost, the overall reliability of the model being attributed to its physical soundness and proved only heuristically. On the other hand, this approach is very low demanding of computing power and, therefore, it favors the rush toward those large-scale simulations actually needed in the realm of solid mechanics and/or in the multiscale paradigm. As a consequence, in the last decade or so very many atomistic simulations based on empirical potential have been performed, addressing different nanomechanics problems (with a preference for fracture-related phenomena).

In general, atomistic simulations – whether well planned and performed – provide a body of knowledge consistent with solid mechanics. However, at variance with continuum theory, they do not need any initial guess for the constitutive stress-strain relation underlying the mechanical response: in fact, the actual behavior is obtained directly from the collective response of the interacting atoms. Under this respect, they can be considered as a first principles mechanical theory. In addition, these simulations can predict possible intriguing new features occurring at the very atomic scale. Here classical solid mechanics cannot be easily applied either because the continuum concept is no longer a valid one, and because elastic fields are often mathematically singular at this scale (we refer, for instance, to the stress field at the tip of a crack in a brittle material). In conclusion, atomistic simulation have established as an essential and important research tool in modern nanomechanics.

This review is addressed to discuss the basic concepts and the methods underlying atomistic simulations. Their formal structure and some detail about their numerical implementaion is given in Sec.2. We then discuss the fundamental requirements that must be satisfied by any “trustworthy interatomic potential” for applications in nanomechanics in Sec.3, where continuum theory will be used as a conceptual guideline. The following Sec.4 will thoroughly describe the actual procedure to generate a many-body, computationally efficient and quantitatively accurate interatomic potential. Finally, Sec.5 will outline some recent investigation on the failure strength of nanostructured brittle materials.

2. Atomistic simulations: The basic conceptual framework

2.1. Atom dynamics

The total force $\vec{F}_i$ acting on the *i*-th atom of an *N*-particle system is given by

$$\vec{F}_i = -\vec{\nabla}_i U(\vec{r}_1, \vec{r}_2, \cdots, \vec{r}_N) \tag{2.1}$$

where $U(\vec{r}_1, \vec{r}_2, \cdots, \vec{r}_N)$ is the potential - depending only upon atomic positions – acting among the *N* particles and $\{\vec{r}_i\}_{i=1,\cdots N}$ are their potisitions. From eq.(2.1) the trajectories

$$\vec{r}_i = \vec{r}_i(t) \tag{2.2}$$

can be computed, provided that the instantaneous positions are computable at each time *t*.

In order to put eq.(2.2) into a form suitable for digital computers, we need to introduce the discretization of the time evolution. This is obtained by defining a suitable time-step δt, representing the unit of time interval, and by further assuming that the force $\vec{F}_i$ is constant over δt. Accordingly, the time evolution ($t \rightarrow t+\delta t$) of the atomic positions and velocities is obtained by solving the equations of motion through finite-difference algorithms [4,5]. Typically, we set $\delta t = 10^{-15}$s.

For investigations addressed to solid mechanics the above procedure – which is generally named *molecular dynamics* (MD) – is typically implemented at zero-temperature. Under this assumption, it is more efficient to rather adopt the two-step *dumped dynamics* (DD) method. Once that the system is loaded, the resulting equilibrium atomic positions are found through a two-step procedure: at first, the atomic positions and velocities are updated over the time interval ($t \rightarrow t+\delta t$) using ordinary finite-difference algorithms; then, the atomic velocity vectors $\vec{V}_i$ are set to zero for those atoms fulfilling the following relation

$$\vec{F}_i \cdot \vec{r}_i \leq 0 \tag{2.3}$$

The key-idea of the DD method is that an atom is allowed to accelerate towards a minimum of configurational energy, while it is stopped when it attempts to escape from such a minimum-energy basin. The DD algorithm is iterated until the maximum atomic force is smaller than a suitable threshold, which is typically set to 10^{-4} eV/Å.

Following the DD protocol, we can define an elementary (but good enough for mechanical investigations) *iterative scheme*, able to generate the evolution of the simulated sample under a system of forces, including possible external ones: given an initial configuration (i.e.: the loads on the body; the geometry and shape of the mechanical defects like, e.g., cracks, voids or inclusions; and the positions of the atoms forming the body), atomic forces are computed and atomic positions accordingly updated; the new configuration is used as input for the next force calculation, and so on. The procedure is iterated until the convergence threshold is eventually reached: the corresponding atomic configuration will represent the equilibrium one for the system under investigation and under the assigned loading condition. At this stage any mechanically-relevant quantity (like, e.g., strain and stress fields) can be calculated.

2.2. Interatomic potentials

The most computationally intensive step is most likely the calculation of interatomic forces, i.e. the numerical solution of eq.(2.1). We need, therefore, to minimize the number of force calls at each loop of the DD method. For this reason, short-ranged potentials are especially well suited for applications to systems containing a large number of atoms. In most relevat cases, it is in fact possible to exclude from the interaction list of any atom i those particles $j \neq i$ found at distances larger than a suitably-defined potential cut-off [6]. Being a key issue of atomistic simulations, we will provide some more detail about the interactomic potential.

A good interaction model $U(\vec{r}_1, \vec{r}_2, \cdots, \vec{r}_N)$ should provide an accurate estimation of total energy and related quantities (e.g. its derivatives), as well as it should be physically sound, i.e. it must be firmly rooted into a rigorous description of fundamental interactions. Only the occurrence of such features does provide a predictive and transferable model for meaningful simulations [6].

The simplest possible approach to elaborate a theory for $U(\vec{r}_1, \vec{r}_2, \cdots, \vec{r}_N)$ consists in formally expanding the total potential into a series of two-body $U^{(2)}$, three-body $U^{(3)}$, ... n-body $U^{(n)}$ terms

$$U(\vec{r}_1, \vec{r}_2, \cdots, \vec{r}_N) = \sum_{i>j} U^{(2)}(\vec{r}_i, \vec{r}_j) + \sum_{i>j>k} U^{(3)}(\vec{r}_i, \vec{r}_j, \vec{r}_k) + \cdots \tag{2.4}$$

and by arresting the expansion at a given order, as guessed by the chemical nature of the underlying bond network or just by ease of implementation or numerical convenience. When atomistic simulations are applied to solid mechanics, special attention must be devoted to the criteria for truncating the

expantion given in eq.(2.3). The simplest possible choice, i.e. using just two-body interaction potential, could in fact lead to results in contraddiction to continuum mechanics, or even to wrong concepts. This issue is extensively treated in Sec.3.

In addition to the above problem, we remark that each functional $U^{(i)}$ depends upon empirical parameters that need to be fitted once for all onto a suitable database of system properties [6]. The empirical character of $U(\vec{r}_1,\vec{r}_2,\cdots,\vec{r}_N)$ dramatically improves the overall numerical efficiency of the simulation, allowing for simulations up to millions of particles. Unfortunately, the very same empirical character also limits (sometimes even severely!) the transferability of the potential itself. In order to overcome this limitation, we could develop a potential theory at the more fundamental quantum level, which, however, falls beyond the scope of the present paper. We simply remark that the quantum mechanical description of atom-atom interactions, although superior as far as the accuracy and transferability are concerned, is characterized by a heavy computational workload which practically prevents the use of quantum simulations in the realm of solid mechanics.

2.3. Atomic stress

While the displacement and strain fields of continuum mechanics have a natural counterpart in atomistic theory (they are simply computed as a difference from the initial and final atomic positions), the stress field deserves a more careful definition and handling.

The atomic-level expression (the so-called *virial* of the forces) for the stress tensor $\sigma_{\alpha\beta}$ of a system under a generic deformation state described by the strain tensor $\varepsilon_{\alpha\beta}$ (see below, eq.(3.5)) at T=0K is defined as [4]:

$$\sigma_{\alpha\beta} = \frac{1}{\Omega}\frac{\partial U}{\partial \varepsilon_{\alpha\beta}} \tag{2.5}$$

where hereafter α,β are the cartesian components, Ω is the system volume, and U is the internal energy as defined by the interatomic potential. By means of eqs.(2.4) and (2.5) we can get an expression for the stress-tensor in terms of a sum over on-site contributions U_i

$$\sigma_{\alpha\beta} = \frac{1}{N\omega}\sum_i \frac{\partial U_i}{\partial \varepsilon_{\alpha\beta}} \tag{2.6}$$

provided that we attribute to any atom the same average volume $\omega=\Omega/N$. Although this assumption is widely used, it should be nevertheless noted that it

is in principle correct only for *homogeneous* systems. Actually, many interesting problems in modern nanomechanics refer to systems that do not fulfill such an assumption. Therefore, we need to better refine the volume concept. A possible solution is offered by a volume discretization procedure at the region of interest: we can divide the total available space into elementary volumes; then, each elementary volume is uniquely assigned to its next neighbor atom site. The *atomic volume* of any given lattice site is finally defined as the sum of the elementary volumes attributed to that atom site. It can be proved that such a discretization procedure is basically equivalent to the Voronoi tessellation, it is unique, and it unambiguously attributes to each atom a proper value of the volume. Furthermore, it is valid even in the case of convex, but not homogeneous systems [7].

The most rigorous atomic-level stress formulation can be eventually cast in the form

$$\sigma_{\alpha\beta} = \frac{1}{N}\sum_i \frac{1}{\omega_i}\frac{\partial U_i}{\partial \varepsilon_{\alpha\beta}} = \frac{1}{N}\sum_i \sigma_{\alpha\beta,i} \tag{2.7}$$

For any pair (*i*,*j*) of next neighboring atoms we further calculate the bond stress

$$\overline{\sigma}_{\alpha\beta}(x,y,z) = \frac{1}{2}\left(\sigma_{\alpha\beta,i} + \sigma_{\alpha\beta,j}\right) \tag{2.8}$$

and we attribute it to the average atomic position of the selected atom pair. We will refer to such a quantity as the *local stress tensor*. This atomic-level quantity can be directly compared to the macroscopic stress field calculated in the context of linear elastic fracture mechanics.

Finally, we remark that the state of deformation assigned as initial condition to the simulation cell is maintained by means of the *constant-traction method* [8]. According to this method, mode-I loading can be reproduced by removing the periodic boundary conditions along, say, the *z*-direction, while preserving the periodicity along *x* and *y*. The resulting free surfaces (normal to the *z* axis) are pulled - in addition to ordinary atomic force actions - by constant tractions aimed at mimicking the embedding into an infinite strained bulk at the selected state of loading. The value of the traction $\boldsymbol{t}_i$ on each atom at the free (non-periodic) surface can be shown to be exactly equal to the opposite of the restoring force $\boldsymbol{f}_i$ from the empty space across the free border [8]

$$t_i^{\alpha} = \int_{\Delta S}\left(\sigma_{\alpha\beta}^{i}\cdot n^{\beta}\right)dS = -f_i^{\alpha} \tag{2.9}$$

where **n** is the unit vector (locally and instantaneously) perpendicular to the free-surface element ΔS centered around the atom i. Note that for the numerical evaluation of the traction it is not necessary to explicitly calculate the stress tensor, therefore the definition (2.8) gets around the problem of defining a proper local atomic volume.

3. Atomistic description of solid mechanics

3.1. Introduction and historical background

The formal structure of the elasticity theory from the atomistic (or molecular) point of view represents a crucial issue, largely addressed in the scientific literature since the first attempts to model the mechanical behavior of the elastic (or deformable) bodies. During the XIX century, different approaches have been introduced in order to model the elastic behavior of the solid media. Firstly, Fresnel [9] and Navier [10] published, respectively in 1820 and 1821, very similar results based on the so-called *corpuscular approach*; they systematically adopted the Lagrange "Mécanique analytique", describing the motion of an elastic solid decomposed into a given collection of point masses interacting by means of distance-varying elastic forces. This approach does not consider the modern concept of stress because the forces are transmitted at molecular level only. On the contrary, in 1822, Cauchy [11] introduced the continuum approach to study the elastic properties of the solid bodies. In such a theory, he obtained the equilibrium equations exactly in the same form in which they appear in modern textbooks: therefore, he defined a sort of tensorial pressure (stress) and he stated that the stress tensor divergence is zero (at equilibrium and in absence of volumetric external forces). Moreover, in 1828, Cauchy [12] introduced the linear constitutive relations (the Hooke law) defining two different elastic constants needed to model the isotropic media.

Despite several efforts, the problem of reconciling the opposing molecular and the continuum approaches remained a very intriguing challenge for many years. The simplest molecular models - including only central two-body interactions - describe the mechanical behavior of any material by means of a single elastic constant, a sort of *scalar stiffness*. At variance, the continuum approach predicts in the isotropic case the need of two independent and material-specific parameters. So, the basic question is: do we need just one or actually two elastic modulus(i) to properly describe elastic isotropic media?

The first robust attempt to answer to this problem has been given by Voigt [13]: according to his model, the regular structure of a crystal suggests that, when a molecule (or atom) is added to the lattice, an *ad hoc* couple of forces acts on the molecule in order to set its correct orientation within the crystal. According to the modern terminology, we can say that such a molecular torque

could correspond to an effective many-body interaction, at work among the elementary constituents of the lattice. Voigt, by considering both the central forces and the three-body interactions (i.e. the simplest effective molecular torques), obtained the general equations of the elasticity theory for isotropic solids containing two independent constants, as predicted by continuum approach and consistently with experimental knowledge.

Many other crucial developments have been performed during the XIX century: Poisson and Saint-Venant confirmed and extended several molecular elasticity results; Green and Thomson introduced the energetic and the thermodynamic concepts in the continuum approach. In Italy Castigliano, Betti and Beltrami formalized the theory from the mathematical point of view and found out several theoretical and applied methods, mainly based on the potential theory [14]. A complete narration about the history of the elasticity theory falls beyond the scope of the present work and can be found elsewhere [15].

Although this subject has been widely investigated in the past, the connection between the continuum and the atomistic approaches remains a topic of crucial importance also in present-day material science. In particular, some modern developments are useful in order to correctly derive the interaction force model to be used in atomistic simulations. In next Sections we analyze three paradigmatic important cases, namely:

i. two-dimensional hexagonal crystal (triangular isotropic lattice) with two-body interactions (see Section 3.3);
ii. two-dimensional hexagonal crystal (triangular isotropic lattice) with two-body and three-body interactions (see Section 3.4);
iii. two-dimensional square crystal (square anisotropic lattice) with two-body and three-body interactions (see Section 3.5).

Such examples should be important in order to improve the potentials adopted in atomistic simulations for solving solid mechanics problems. The conclusions will be of general validity, although our arguments are developed, for sake of simplicity, for 2-dimensional crystals only.

3.2. Two-body and three-body interactions

In this Section we throughly discuss two-body and three-body interactions between/among atoms in a crystalline structure. We point out that in this discussion we do not specify any particular crystal lattice, focusing solely on the effective modeling of the chemical bonds.

We begin by taking into consideration an arbitrary lattice of point masses which interact through simple central forces (two-body interaction), acting between nearest neighbors only. We focus on a pair of particles placed in

positions $\vec{r}_1^{(0)}$ and $\vec{r}_2^{(0)}$ at equilibrium or, equivalently, in a configuration of minimum energy. If a small deformation is applied, the new positions will be given by

$$\vec{r}_i = \vec{r}_i^{(0)} + \vec{u}\left(\vec{r}_i^{(0)}\right) \tag{3.1}$$

where we have introduced the displacement vector field $\vec{u}\left(\vec{r}_i^{(0)}\right)$ defined for any equilibrium position in the lattice. We point out that this simple definition is central to the atomistic description of the classical fields used in the continuum theories.

We further assume that the two-body interaction may be represented by a force linearly varying with the distance between the atoms, i.e. by an effective spring. Indeed, by taking advantage of the small displacement hypothesis, we can say that the linear approximation corresponds to the expansion of the interaction potential in a Taylor series centered in the minimum-energy configuration, truncated just at the first (quadratic) non-zero term. Therefore, the spring constant K_s can be evaluated as the second derivative of potential energy with respect to distance.

If the particles in $\vec{r}_1$ and $\vec{r}_2$ are nearest neighbors, the force on the first particle due to the second one is

$$\vec{F}_1 = k_s \hat{n}\left(\left|\vec{r}_2 - \vec{r}_1\right| - l\right) \tag{3.2}$$

where $l = \left|\vec{r}_2^{(0)} - \vec{r}_1^{(0)}\right|$ is the equilibrium distance and $\hat{n}$ is the unit vector in the direction of the central force (see Fig. 1 for details).

By adopting eq.(3.1) and by assuming slow variations of the displacement on the atomic scale, we can expand this force up to the first order in the difference $\vec{u}\left(\vec{r}_2^{(0)}\right) - \vec{u}\left(\vec{r}_1^{(0)}\right)$. Then, writing

$$\vec{u}\left(\vec{r}_2^{(0)}\right) \approx \vec{u}\left(\vec{r}_1^{(0)}\right) + \left[\frac{\partial \vec{u}}{\partial \vec{r}}\right]\left(\vec{r}_2^{(0)} - \vec{r}_1^{(0)}\right) \tag{3.3}$$

we obtain

$$\vec{F}_1 \approx k_s l \hat{n}\left(\hat{n} \cdot \left[\frac{\partial \vec{u}}{\partial \vec{r}}\right]\hat{n}\right) \tag{3.4}$$

where we have introduced the jacobian matrix $\left[\partial \vec{u} / \partial \vec{r}\right]_{\alpha\beta} = \partial u_\alpha / \partial r_\beta$. Finally, defining the symmetric *strain tensor*

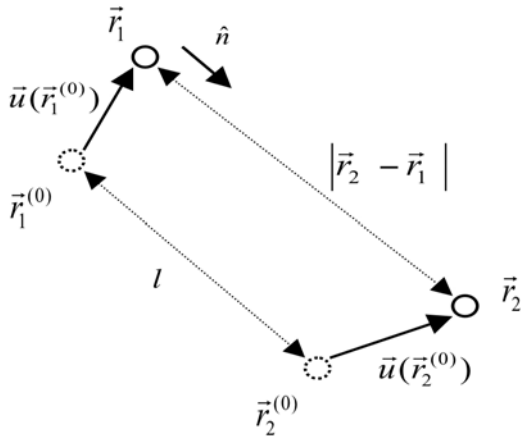

Figure 1. Displacement and distance vectors for a pair of atoms, before and after deformation. The unit vector $\hat{n}$ in the direction of the central force is shown as well.

$$\varepsilon_{\alpha\beta} = \frac{1}{2}\left(\frac{\partial u_\alpha}{\partial r_\beta} + \frac{\partial u_\beta}{\partial r_\alpha}\right) \tag{3.5}$$

we find

$$\vec{F}_1^{\,2B} \approx k_s l \hat{n}\left(\hat{n} \cdot \vec{\varepsilon}\,\hat{n}\right) \tag{3.6}$$

This is the force acting on a given particle caused by a neighboring atom, placed at distance l and aligned in direction $\hat{n}$, when the local deformation is characterized by the strain tensor $\vec{\varepsilon}$. In order to compute the total force applied to a single atom, we have to choose a microscopic crystal structure, as shown in the next Sections.

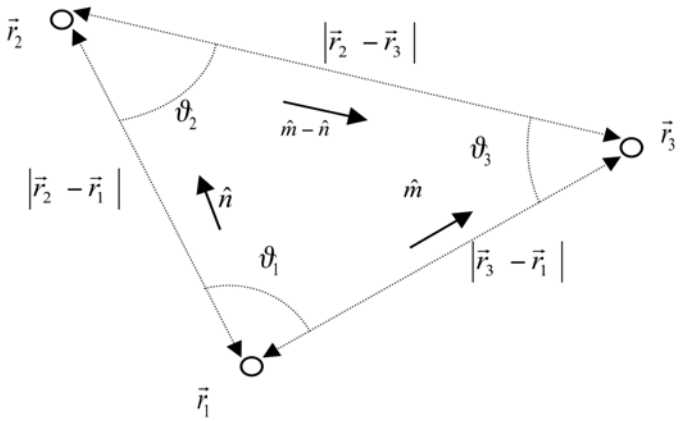

Figure 2. Distances and angles for a three-atom cluster. The unit vectors $\hat{n}$ and $\hat{m}$ in the direction of the central forces are shown as well.

We now take into consideration a three-body interaction among nearest neighbors. In this case we begin by defining a potential function involving three atomic positions $\vec{r}_1$, $\vec{r}_2$ and $\vec{r}_3$. We assume that the three angles ϑ_1, ϑ_2 and ϑ_3 (see Fig. 2) are respectively equal to α_1, α_2 and α_3 at equilibrium. Therefore, we can choose a potential energy of the form

$$U^{3B} = \frac{1}{2}\left\{H_1\left[\cos(\vartheta_1)-\cos(\alpha_1)\right]^2+ H_2\left[\cos(\vartheta_2)-\cos(\alpha_2)\right]^2+ H_3\left[\cos(\vartheta_3)-\cos(\alpha_3)\right]^2\right\} \quad (3.7)$$

where H_1, H_2, H_3 are suitable constants. Eq.(3.7) governs the behavior of the angles ϑ_1, ϑ_2 and ϑ_3 between atoms and it has the following main property: the minimum value (U^{3B}=0) is reached only when $\vartheta_i = \alpha_i$ for i=1,2,3. Since we want to study the case of a triangular lattice, we take into consideration the following additional hypothesis: the three equilibrium angles are given by $\alpha_1 = \alpha_2 = \alpha_3 = \pi/3$; therefore, we may write

$$U^{3B} = \frac{1}{2}hl^2\left\{\left[\cos(\vartheta_1)-\frac{1}{2}\right]^2+\left[\cos(\vartheta_2)-\frac{1}{2}\right]^2+\left[\cos(\vartheta_3)-\frac{1}{2}\right]^2\right\} \quad (3.8)$$

where we have let H_1=H_2=H_3=hl^2, being l the inter-atomic distance in the unstrained lattice. In such a way, the constant k_s (describing the two-body interactions) and the constant h (describing the three-body interactions) usefully assume the same physical units.

By applying the same approximations used to derive eq.(3.6), we find the following net force on atom 1

$$\vec{F}_1^{\,3B} \approx \frac{3}{2}hl\left\{\left(\hat{m}\cdot\vec{\varepsilon}\hat{n}+\frac{1}{2}\hat{m}\cdot\vec{\varepsilon}\hat{m}-\hat{n}\cdot\vec{\varepsilon}\hat{n}\right)\hat{m}+\left(\hat{m}\cdot\vec{\varepsilon}\hat{n}+\frac{1}{2}\hat{n}\cdot\vec{\varepsilon}\hat{n}-\hat{m}\cdot\vec{\varepsilon}\hat{m}\right)\hat{n}\right\} \quad (3.9)$$

where $\hat{m}$ and $\hat{n}$ are the unit vectors defined in Fig. 2. In order to give an explanation of this equation, we remark that the bilinear form $\hat{m}\cdot\vec{\varepsilon}\hat{n}$ is directly connected to the variation of the angle between the directions $\hat{m}$ and $\hat{n}$ induced by the deformation described by $\vec{\varepsilon}$. As expected, the force term given in eq.(3.9) depends on the angular distortion of the triangle represented in Fig. 2. Moreover, we can say that if ϑ_2 and ϑ_3 are equal, then the force is oriented along the bisector of the angle ϑ_1 in such a way to increase ϑ_1 if $\vartheta_1 < \pi/3$ and to decrease ϑ_1 if $\vartheta_1 > \pi/3$.

Another important example of three-body interactions is that describing a cubic crystal (or, equivalently, its 2-dimensional version). By considering the

simple case of a planar square lattice, we may obtain the corresponding equations by letting $\alpha_1 = \alpha_2 = \alpha_3 = \pi/2$ in eq.(3.7) (of course, in this case, the triangle shown in Fig. 2 should be replaced by a square). The three-body potential energy reduces to

$$U^{3B} = \frac{1}{2} hl^2 \left[\cos^2(\vartheta_1) + \cos^2(\vartheta_2) + \cos^2(\vartheta_3)\right] \tag{3.10}$$

where, once again, we have let $H_1=H_2=H_3=hl^2$, being l the lattice constant. Therefore, the expression

$$\vec{F}_1^{\,3B} \approx 4hl(\hat{m} \cdot \vec{\vec{\varepsilon}}\,\hat{n})(\hat{n} + \hat{m}) \tag{3.11}$$

directly provides the force on atom 1.

3.3. Triangular lattice with central forces only

In this Section we derive the balance equation of continuum mechanics for isotropic media, in the simple case of pure central forces and in the linear regime approximation given by eq.(3.6). Under such hypothesis, we have to choose an isotropic 2-dimensional crystal: as a matter of fact, the only crystalline isotropic structure in two dimensions is the regular triangular lattice shown in Fig 3.

Any particle has six nearest neighbors placed at distance l (equal to the edge of the triangular mesh). By computing the force due to the opposite neighbors A and B of atom 1, we find

$$\vec{F}_{1,AB}^{\,2B} = k_s l \hat{n} \cdot (\vec{\vec{\varepsilon}}_A - \vec{\vec{\varepsilon}}_B)\hat{n} \tag{3.12}$$

where we used eq.(3.6) and we indicated the unit vector connecting A to B with $\hat{n}$. The total force on atom 1 is given by the sum of three terms similar to eq.(3.12) (calculated, respectively, along the three directions A-B, C-D and E-F shown in Fig. 3). Now, in order to give a continuum description of the system, we have to divide the total force by the area occupied by each atom, i.e. by $S = l^2\sqrt{3}/2$. The resulting force density is

$$\vec{f}_{1,AB}^{\,2B} = \frac{2\sqrt{3}}{3} k_s \,\hat{n} \cdot \frac{(\vec{\vec{\varepsilon}}_A - \vec{\vec{\varepsilon}}_B)}{l} \hat{n} \tag{3.13}$$

The ratio $\frac{1}{l}(\vec{\vec{\varepsilon}}_A - \vec{\vec{\varepsilon}}_B)$ in eq.(3.13) can be identified with the projection $(\hat{n} \cdot \partial/\partial\vec{r})\vec{\vec{\varepsilon}}$ of the gradient of the strain tensor. With this insight, the total force due to the couple *AB* becomes

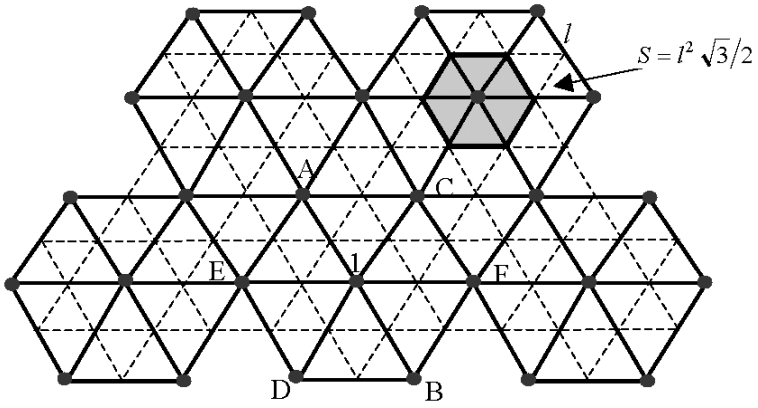

Figure 3. Planar (2-dimensional) triangular crystale with lattice constant l. One can easily find the area S of the unit cell and the first neighbors (A, B, C, D, E, and F) of the atom 1.

$$\vec{f}_{1,AB}{}^{2B} = \frac{2\sqrt{3}}{3} k_s \, \hat{n} \cdot \left(\hat{n} \cdot \partial / \partial \vec{r}\right) \vec{\varepsilon} \hat{n} \tag{3.14}$$

Finally, the Newton law describing the motion atom 1 is obtained as follows

$$\vec{f}_{1,AB}{}^{2B} + \vec{f}_{1,CD}{}^{2B} + \vec{f}_{1,EF}{}^{2B} + \vec{b} = \rho \ddot{\vec{u}} \tag{3.15}$$

where $\vec{b}$ is the density of external forces applied to the system, ρ is the mass density and $\ddot{\vec{u}}$ is the acceleration. Each of the force terms in eq.(3.15) can be developed through the eq.(3.14), leading to the final elasticity equation

$$\frac{\sqrt{3}}{4} k_s \left[\nabla^2 \vec{u} + 2\nabla\left(\nabla \cdot \vec{u}\right) \right] + \vec{b} = \rho \ddot{\vec{u}} \tag{3.16}$$

This is the main result of this Section, describing the linear elastic behavior of a planar triangular lattice governed by purely central forces.

It is interesting to draw a comparison with the standard results of continuum mechanics for isotropic solids. We remind that the displacement equation derived from continuum is

$$\mu \nabla^2 \vec{u} + \left(\lambda + \mu\right) \nabla\left(\nabla \cdot \vec{u}\right) + \vec{b} = \rho \ddot{\vec{u}} \tag{3.17}$$

where λ and μ are the Lamé material-specific constants. The comparison between eqs.(3.16) and (3.17) provides the effective elastic moduli of the triangular lattice

$$\lambda = \mu = \frac{\sqrt{3}}{4} k_s \tag{3.18}$$

or, equivalently, its Young modulus and the Poisson ratio

$$E = \frac{5\sqrt{3}}{8} k_s \quad \text{and} \quad \nu = \frac{1}{4} \tag{3.19}$$

Eqs.(3.18) and (3.19) prove that an atomistic model for the triangular lattice with central forces only is not able to take into account all the elastic features predicted by the continuum elastic theory (and confermed experimentally). In particular, eq.(3.18) indicates that, according to this model, the material should have only one characteristic elastic constant, while eq.(3.19) implies that it should exist a universal value of the Poisson ratio, independent on the actual physical properties of the material.

3.4. Triangular lattice with two-body and three-body interactions

We now extend the case study investigated in the previous Section (see Fig. 3) to including three-body interactions as well. By adopting the angular dependent force defined in eq.(3.9), we can itemize the full set of forces at work as follows:

- two-body interaction forces, as given in eqs.(3.14) and (3.15);
- three-body interaction forces. For instance, six angular contributions are working on atom 1 of Fig. 3, as calculated in eq.(3.9): they correspond to the angles A1C, C1F, F1B, B1D, D1E and E1A.
- the external forces applied to the lattice.

Following the same procedure outlined in the previous Section, we get

$$\frac{3}{4}\left(\frac{\sqrt{3}}{3} k_s + \frac{9}{4} h\right) \nabla^2 \vec{u} + \frac{\sqrt{3}}{2} k_s \nabla\left(\nabla \cdot \vec{u}\right) + \vec{b} = \rho \ddot{\vec{u}} \tag{3.20}$$

We can draw a comparison with the continuum version, eq.(3.17), finding the effective elastic moduli of the lattice

$$\lambda = \frac{3}{4}\left(\frac{\sqrt{3}}{3} k_s - \frac{9}{4} h\right) \quad \text{and} \quad \mu = \frac{3}{4}\left(\frac{\sqrt{3}}{3} k_s + \frac{9}{4} h\right) \tag{3.21}$$

or, equivalently, the Young modulus and the Poisson ratio

$$E = \frac{3\sqrt{3}}{8} k_s \left(\frac{\sqrt{3}}{3} + \frac{9}{4}\frac{h}{k_s} \right) \left(\frac{5\sqrt{3}}{3} - \frac{9}{4}\frac{h}{k_s} \right) \quad \text{and} \quad \nu = \frac{1}{4} - \frac{9\sqrt{3}}{16}\frac{h}{k_s} \tag{3.22}$$

In conclusion, only this improved lattice model can correctly describe the elastic behaviour of any isotropic media, since it provides the atomistic expression for *both independent* elastic constants. In other words, we can state that at least three-body interactions are indeed mandatory in order to accurately reproduce the complex mechanical behaviour of real isotropic materials. This feature will be extensively used in the next Section.

Finally, we introduce some energetic considerations. It is well known that the elastic moduli must fulfil some restrictions, due to thermodynamic reasons. More precisely, the Lamé constants must obey the inequalities $\mu > 0$ and $(2\mu+3\lambda) > 0$. On the other hand, the Poisson ratio ν and Young modulus E satisfy the relations $-1 < \nu < 1/2$ and $E > 0$, respectively [16]. Consequently, the interaction parameters k_s and h must be as follows

$$k_s > 0 \quad \text{and} \quad -\frac{4\sqrt{3}}{27} k_s < h < \frac{20\sqrt{3}}{27} k_s \tag{3.23}$$

When h approaches the value $-4\sqrt{3}k_s/27$, the Poisson ratio becomes equal to 1/2 (a situation found in rubbery materials): the system is *volume* (*area*) *preserving* since the three-body interactions are working contrarily (h <0) to what expected. In fact, when a given angle differs from its equilibrium value, the three-body forces operate in the direction of bringing the system as far as possible from the equilibrium. In other words this three-body contribution makes the system mechanically unstable (of course, the sum of the two-body and the three-body contributions is always stabilizing under the condition given in eq.(3.23)). On the other hand, when h approaches the value $20\sqrt{3}k_s/27$, the Poisson ratio has negative value -1 (a situation common in some *re-entrant polymer foams*): in this case the structure is *shape preserving*, allowing only deformations described by isotropic rescaling of the body. This happens because of the large value assumed by the angular stiffness h.

3.5. Square lattice

We now turn to considering the square lattice shown in Fig. 4. We are interested in this (particularly simple) anisotropic material since we want to prove that also in this case the three-body interactions are indeed necessary to fully describe elasticity, as previously found for the isotropic case. For further convenience, we remind that in continuum mechanics a cubic crystal (as well as its planar 2-dimensional counterpart) is described by three independent

elastic constants, namely C_{11}, C_{12} and C_{44}. The definition of such constants is based on the stress-strain constitutive relations: $T_{xx} = C_{11}\varepsilon_{xx} + C_{12}\varepsilon_{yy}$, $T_{yy} = C_{12}\varepsilon_{xx} + C_{11}\varepsilon_{yy}$ and $T_{xy} = C_{44}\varepsilon_{xy}$, where $T_{\alpha\beta}$ are the components of the stress tensor (please note the the above constitutive relations are written for a 2-dimensional body under plain strain border conditions).

In the present case the forces working on atom 1 can be summarized as follows (see Fig. 4 for details):

- two-body interaction forces acting between the first neighbors A, B, C and D, described by eq.(3.6) with spring constant k_s and interaction distance l;
- two-body interaction forces acting between the second neighbors E, F, G and H, described by eq.(3.6) with spring constant k_d and interaction distance $\sqrt{2}l$;
- three-body interaction forces (constant h). Four contributions are working on atom 1 of Fig. 4, as calculated in eq.(3.11); they correspond to the agles A1B, B1C, C1D and D1A;
- the external forces applied to the lattice.

The balance equation leads to

$$\begin{cases} (k_s + k_d)\dfrac{\partial^2 u_x}{\partial x^2} + 2(k_d + 2h)\dfrac{\partial^2 u_y}{\partial x \partial y} + (k_d + 4h)\dfrac{\partial^2 u_x}{\partial y^2} + b_x = \rho \ddot{u}_x \\ (k_s + k_d)\dfrac{\partial^2 u_y}{\partial y^2} + 2(k_d + 2h)\dfrac{\partial^2 u_x}{\partial y \partial x} + (k_d + 4h)\dfrac{\partial^2 u_y}{\partial x^2} + b_y = \rho \ddot{u}_y \end{cases} \tag{3.24}$$

A comparison with the results of the continuum mechanics for cubic anisotropic systems allows us to find a direct relationship between the elastic constants and the atomistic parameters

$$\begin{cases} C_{11} = k_s + k_d \\ C_{12} = k_d \\ C_{44} = 2(k_d + 4h) \end{cases} \Leftrightarrow \begin{cases} h = \dfrac{1}{8}(C_{44} - 2C_{12}) \\ k_s = C_{11} - C_{12} \\ k_d = C_{12} \end{cases} \tag{3.25}$$

Such relations demonstrate that three kinds of forces (corresponding to the materials parameters k_s, k_d and h) are indeed necessary for correctly modeling the elastic behavior of the cubic crystal, at least under the assumption of small deformations. In addition, the second set of formulas in eq.(3.24) could be

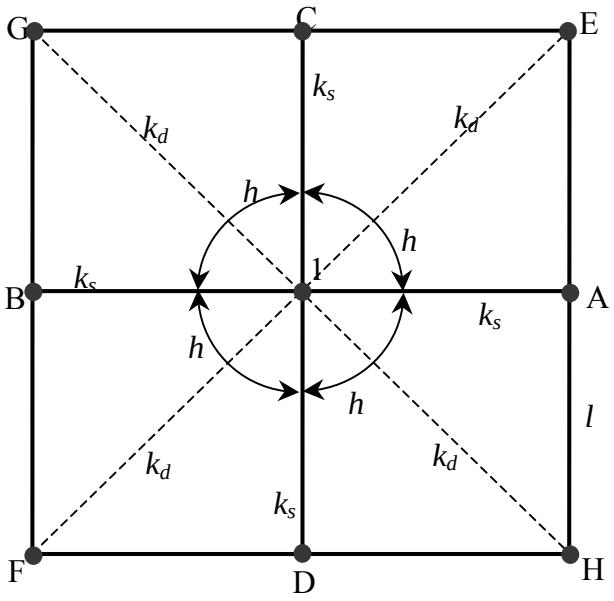

Figure 4. Portion of a planar square lattice with inter-atomic distance l. The arbitrary atom 1 interacts with the crystal by means of three kinds of forces: spring-like forces (constant k_s) with atoms ABCD, spring-like forces (constant k_d) with atoms EFGH and angular dependent forces which tends to maintain right the angles A1C, A1D, B1D and C1B.

useful to fit the atomistic force model onto the experimentally-known elastic constants. It is also useful to remark that the elastic constants are subjected (in cubic symmetry) to the thermodynamic restrictions: $C_{11} > 0, C_{44} > 0$ and $-C_{11}/2 < C_{12} < C_{11}$. They have the following implications on the atomistic parameters: $k_s + k_d > 0$, $k_d + 4h > 0$, $k_s + 3k_d > 0$ and $k_s > 0$, which must be always verified to obtain a physically stable material. Interesting enough, this case study shows that the range of interactions at the atomic scale cannot be restricted just to the first neighbors in the general case of anisotropic materials. This feature will be extensively discussed in the next Section.

Finally, it is noteworthy the fact that also an isotropic material can be represented by the square lattice model. As a matter of fact, by imposing the isotropy Cauchy relation C_{44}=C_{11}-C_{12}, it must hold the relation h =1/8(k_s-2k_d); under this condition, the overall behavior of the square lattice is macroscopically isotropic and only the two coefficients k_s and k_d define the elastic behavior of the system. In such a case it is possible to obtain the Young modulus and the Poisson ratio as follows

$$E = k_s \frac{3k_d + k_s}{2k_d + k_s} \quad \text{and} \quad \nu = \frac{k_d}{2k_d + k_s} \tag{3.26}$$

The above k_s and k_d parameters satisfy the thermodynamic inequalities $k_s + 3k_d > 0$ and $k_s > 0$, assuring the positive definiteness of the potential elastic energy. Therefore, k_d must belong to the interval $(-k_s/3,+\infty)$: the left bound corresponds to $\nu = -1$ and the right one to $\nu = 1/2$. Moreover, if $k_d = 0$, from eq.(3.26), we obtain $E = k_s$ and $\nu = 0$. The zero-value for the Poisson ration is easily justified: with no diagonal springs ($k_d = 0$), a simple traction along a given atomic bond direction cannot induce deformations along the orthogonal direction (lateral restriction).

In conclusion, this Section has outlined a number of important formal properties that an atomistic interaction force model must have in order to be consistent with the elasticity of deformable bodies, as formalized by continuum solid mechanics. This properties will be used in the next Section as a conceptual guideline to work out reliable and accurate potentials. Further discussion about the link between elastic constants and interatomic potentials can be found in Ref.[6].

4. Improved potentials for solid mechanics

4.1. General overview

In order to discuss some vary basic and important features relevant to developing improved potentials for applications in nanomechanics, we will directly refer to the atomistic simulation of brittle fracture in covalent materials (Si, Ge, C, SiC) which turned out to be a very challenging problem: as a matter of fact, most of the available potentials for elemental as well as compound group-IV materials are not able to reproduce the brittle nature of crack propagation [17]. In the case of silicon this holds for the Tersoff potential [18], the Stillinger Weber (SW) potential [19] and the Environment-Dependent Interatomic Potential (EDIP) [20]: all of them predict unphysical behavior during fracture. To our knowledge only a few force models are able to predict the brittle fracture in covalent materials [21, 22, 23]. However, they work just for a specific material and they are not transferable.

By comparing the atomic force provided by SW and EDIP potentials with the Universal Energy Relation (UER) obtained by ab initio calculations [23], Marder et al. [19] concluded that none of the available models for silicon accurately describes the force-separation curve. Such conclusion has been recently supported by the use of pseudopotential method [20, 24]. Several alternative theoretical approaches have been therefore explored in order to study fracture. In the spirit of the multiscale approach, classical force models have been used in combination with other methods [25]. The classical force model is used far from the crack tip, while the chemical bonding nearby the crack tip is described by semiempirical tight-binding [19] or ab initio density functional calculation [26]. Alternatively, the model potential is locally

modified through a learn-on-the-fly procedure [27]. Very recently, it has been also proposed a multiparadigm approach [28] where a reactive force field is applied at the crack tip.

Despite the above considerable effort, the search for simpler model potentials remains open. This is mainly due to the lower computational cost of model potentials with respect to methods involving ab initio or tight binding calculations. By following the general conclusions outlined in the previous Section (namely, the need of many-body interactions and relatively long-ranged forces), it is here investigated how a valid and efficient potential can indeed be generated. The argument is illustrated by using the Tersoff potential as the prototype for interaction models for group-IV materials.

4.2. Universal energy relation

The UER [23] is a two-parameter equation of state describing the variation of the internal energy $U(s)$ of a solid upon the scaled interatomic separation (hereafter referred to as s):

$$U(s) = -E_0(1+s)e^{-s} \tag{4.1}$$

where E_0 is the the cohesive energy per atom (absolute value) and s is

$$s = \left(\frac{r}{r_0} - 1\right)\frac{1}{\mu} \tag{4.2}$$

with r and r_0 being the interatomic distances in the strained and in the equilibrium configuration, respectively. μ is an adimensional parameter measuring the material anharmonicity.

This parameter can be fitted on experiments or ab initio calculations and it can be easily cast in the form

$$\mu = \frac{1}{3}\left(\frac{E_0}{B\omega}\right)^{\frac{1}{2}} \tag{4.3}$$

where ω is the (average) atomic volume and B is the bulk modulus of the material [29]. For the zincblend structure, we have $\omega = \left(2/\sqrt{3}\right)^3 r_0^{\,3}$. In the case of silicon carbide, diamond, silicon and germanium, we calculated μ=0.221, 0.230, 0.205 0.198, respectively. As shown in the following, these relatively large values are not compatible with the (oversimplified) assumption of first-next-neighbor interactions only, consistently with the conclusions of the previous Section.

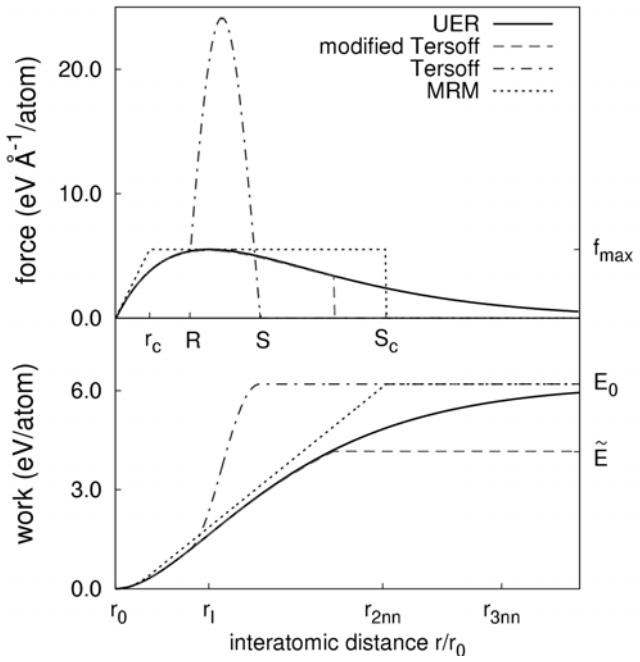

Figure 5. Work (bottom) and force (top) for hydrostatic separation of silicon carbide as a function of the interatomic separation (r/r_0).

The work $W(s)$ necessary to stretch hydrostatically a perfect crystal up to a scaled interatomic distance s is calculated from eq.(4.1) as

$$W(s) = E_0 + U(s) \tag{4.4}$$

The work $W(s)$ is completely controlled by the three constants E_0, μ, r_0 that, in turn, depend on the actual material. For example, the inflection point r_I of the curve $w(s)$ corresponds to $r_I = r_0(1+\mu)$, occurring at $s = 1$. Such an interatomic separation is obtained by spending a work $W(r_I) = (1\text{-}2/e)E_0$ as large as 26% of the total work of separation (per atom) E_0. In Fig. 5 (bottom) the work function $W(s)$ (full line) is represented for the choice μ=0.22, corresponding to the SiC case.

The force $f(s)$ necessary to separate atoms at the interatomic distance s is straightforwardly obtained from $W(s)$

$$f(s) = \frac{dw}{ds} = E_0 \frac{s}{\mu r_0} e^{-s} \tag{4.5}$$

This force is positive in the case of tensile strain ($r > r_0$, i.e. $s > 0$). f is represented in Fig. 5 (top panel) by a full line. The maximum separation force $f_{max} = E_0 (e\mu r_0)^{-1}$ is found to be $r_I = r_0(1+\mu) = 1.44 r_0$, falling within the first

$r_{1nn} = r_0$ and the second $r_{2nn} = 1.633\ r_0$. At distances $r > r_I$ ($s > 1$) the force f decreases as the separation increases. A 90% force reduction (i.e. $f = f_{max}/10$) is observed when $r \sim 2.0 r_0 > r_{3nn} = 1.91\ r_0$. It is important to clarify that the hydrostatic separation energy described by UER does not correspond to any realistic fracture event. Nevertheless, we guess that any force model suitable for fracture must be able to correctly reproduce the UER curve.

4.3. Determining the minimum range for the model potential

The development of a force model with not-too-short range of action is worked out from the corresponding UER by imposing a small number of very fundamental requirements:

i. the force must be a continuous function of strain;
ii. the maximum separation force must be correctly reproduced (i.e. $f^{sr}_{max} = f_{max}$);
iii. the bulk modulus at equilibrium must fit the experimental (or ab initio value);
iv. at tensile strains (up to r_I) the bulk modulus must not increase;
v. the work of separation E_0 must be correctly reproduced.

The condition (ii) is related to the fracture toughness of the perfect material. For instance, if the maximum force is overestimated, the fracture toughness of the material is overestimated as well. Similarly, conditions (iii) and (iv) are needed in order to reproduce the elastic properties of the material. Finally, condition (v) stands for a simple physical requirement: the atomic bonds cannot stiffen during tensile deformation up to the maximum force.

The simplest force model fulfilling the above conditions is represented in Fig. 5 (top panel) as a dotted line. We will refer to such a model as *minimum range model* (MRM). It consists in a linear elastic force over the interval $r_0 \leq r \leq r_c$ (where the bulk modulus is given by the constant value B), while for $r_c \leq r \leq S_c$ the force is constant and equal to the f_{max} value provided by UER. Finally, for any interatomic distance larger than S_c the force is zero. The actual value of r_c is fixed by the intersection between the linear force with slope B, occurring in the region $[r_0, r_c]$, and the constant f_{max}. The parameter S_c is , in turn, fixed by the cohesive energy E_0 [30]

$$S_c = r_0 + r_0\left(e + 0.5e^{-1}\right)\mu \tag{4.6}$$

This value sets the minimum range below which it is not possible to find a force model satisfying the conditions (i)-(v); in other words a model with force extension below S_c is unlikely to describe brittle fracture.

The value S_c/r_0 depends only on the parameter μ characterizing the material. It can be proved that, in the case of covalent group-IV materials, such a minimum value S_c is close to the second nearest neighbor (2nn) distance at equilibrium. In particular, in the case of silicon carbide, it is found that $S_c \approx 1.64\ r_0$ that is slightly larger than second nearest neighbor distance $r_{2nn} \approx 1.15\ r_0$, whereas in the case of silicon and germanium we get $S_c \sim 0.9\ r_{2nn}$. These values suggest that only by taking into account interactions beyond the first neighbor ($\sim r_{2nn}$), it is possible to correctly describe the maximum separation force and, in turn, the fracture toughness of a material. This conclusion, although derived by different arguments, is nicely consistent with the discussion reported in the previous Section.

The minimum range model is indeed a very rough model, its only value being explicatory. In particular, this force model can hardly be used in atomistic simulations. A better device is obtained by multiplying the energy function $U(s)$ by a cutoff function $h(s)$, so as to obtain a new force model $T(s)$

$$T(s) = U(s)h(s) \tag{4.7}$$

The corresponding work separation $W^{sr}(s)$ is modified accordingly

$$W^{sr}(s) = E_0 + T(s) \tag{4.8}$$

and it is (relatively) short ranged as well. An example of such a model is represented as a dot-dashed line in the bottom panel of Fig. 5 where $[R, S]$ is the range where the cutoff $h(s)$ operates. We remark that the cutoff function does not modify the total work of separation, so that condition (v) is satisfied. Furthermore, it does not modify the force field close to the equilibrium distance. Accordingly, conditions (iii), (iv) and (v) are still satisfied by construction. Condition (ii), instead, is satisfied only if the range S of the force model is larger than S_c, according to the previous analysis.

These remarks are valid in general, regardless the actual form of the potential. In particular, they apply to the original Tersoff potential [31] where $S=1.33r_0$, a value much shorter than the 2nn distance. This model is represented in Fig. 5 as dot-dashed line. As expected, the force is overestimated in the range $[R, S]$ and an unphysical peak is observed in the separation force which results four times larger than the correct maximum value f_{max} (Fig. 5, top panel).

The unphysical artifacts due to the imposed severe short rangeness of the interatomic forces prevent the correct description of brittle crack propagation in group IV materials, as shown in Fig. 6 (right panels) where the original Tersoff model was used. In the SiC case (panel A') the crack does not

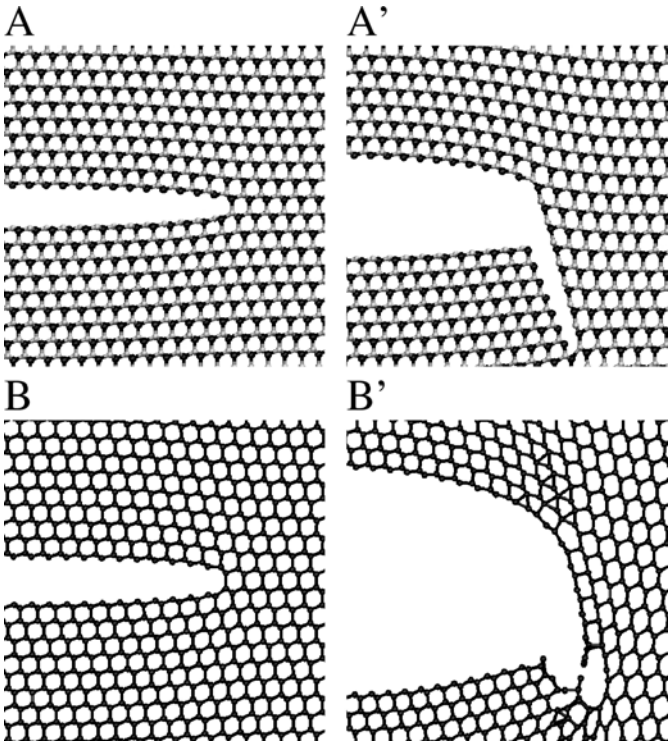

Figure 6. Left panels: artifacts in the crack propagation due to incorrect cutoff force in silicon (top) and silicon carbide (bottom). Right panels: brittle propagation in well reproduced by modified force model.

propagate along the plane of maximum stress (which corresponds to the plane containing the initial crack seed). In the case of silicon (panel B') a plastic accomodation of the stress at the crack tip is even observed, contrary to the brittle nature of this material.

4.4. Improving the force model

Following the above discussion, we introduce an improvement of the Tersoff potential by modifying its cutoff function. The new force model - hereafter labeled as $\tilde{T}$- is represented in Fig. 5 as a dashed line: it extends quite above the equilibrium distance (i.e. it is not restricted just to first next neighbors only), however the cutoff function is step-like. The $\tilde{T}$ model is consistent with the original Tersoff potential when describing systems in condition of low deformation (i.e. when the action of the cutoff function is not involved). For example, all the elastic bulk properties are unchanged. Even the work of separation corresponding to the $\tilde{T}$ model is in very close agreement with the UER curve up to the cutoff. It is, nevertheless, necessary to take into account that the work of separation $\widetilde{E}_0$ is different from E_0. This difference corresponds to the removal of the work done by the cutoff forces and it is

$$\tilde{E}_0 = \int_{r_0}^{\infty} d\tilde{T} < E_0 \tag{4.9}$$

Similarly, the work $\widetilde{\gamma}$ necessary to create new surface during the crack opening is modified with respect to the surface energy value γ.

Notably, such a modified force model is able to reproduce the brittle behavior of group-IV materials, as shown in Fig. 6 for silicon and silicon carbide (panels B and A, respectively). In addition, the calculated failure strength σ_f of cracked systems turns out to be nicely close to the continuum Griffith predictions. This is shown in Fig. 7, where it is reported the failure strength of SiC, Si, Ge and C samples containing a crack of semilength c. The systems were uniaxially loaded along [111] crystallographic direction in all cases. The Griffith curve $\sigma_{LEFM}(c)$ for any material is reported in Fig. 7, as well.

In order to better quantify the difference between the original T and the modified $\widetilde{T}$ Tersoff-like models we have compared the failure strength calculated according to both models. The results for a cracked SiC sample are reported in Fig. 8. Open circles and full diamonds refer to T and $\widetilde{T}$, respectively. We can observe that the original Tersoff model overestimates the failure strength of an amount of about 24-32 GPa with respect to the modified

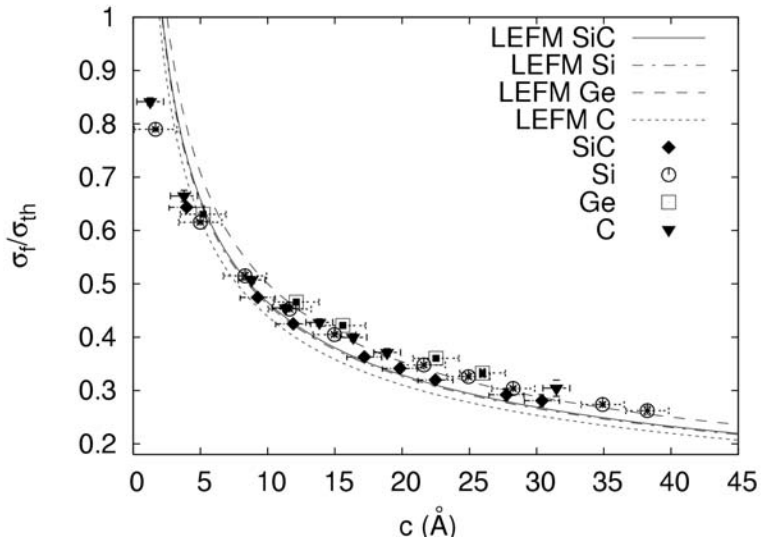

Figure 7. Failure strength σ_f, normalized with respect to the ideal strength σ_{th}, as function of the crack semi-length c. They are reported the results for cracked Si, C, Ge and SiC samples uniaxially loaded along [111] direction. The corresponding linear elastic fracture mechanics (LEFM) curves, obtained with the calculated parameters E and $\widetilde{\gamma}$, are reported as well.

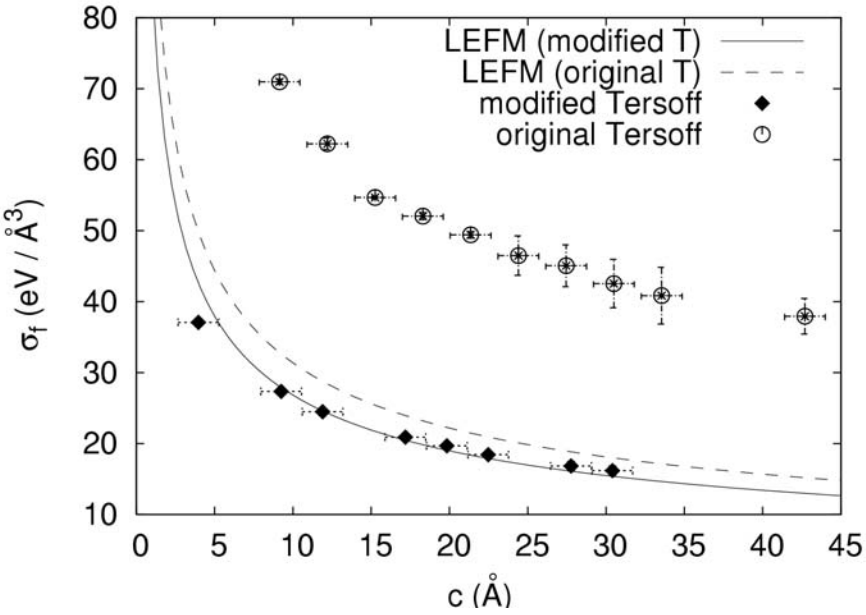

Figure 8. Comparison of the failure strength σ_{th} for a cracked SiC sample, uniaxially loaded along [111] crystallographic direction, calculated according to both original (circle symbols) and modified (diamond symbol) Tersoff model. They are reported also the linear elastic fracture mechanics (LEFM) curves, obtained by using the surface energy calculated according to the original (dashed line) and to the modified (continuum line) Tersoff model.

model. Both results have been compared with the curve obtained within the linear elastic fracture mechanics and calculated using for the surface energy the corresponding values γ (dashed line) and $\widetilde{\gamma}$ (continuous line) for the original and modified potential, respectively. Finally, we observe that the modification of the Tersoff model considerably improves even the ideal strength σ_{th} of perfect C, Si, Ge, SiC crystals (under the condition of uniaxial loading). For the SiC case, in particular, we observe that the calculated strength $\widetilde{\sigma}_{th}$=58±1 GPa is close to the result 50.4 GaP provided by density function theory [32], whereas we get σ_{th}=103±1 GPa by using the original Tersoff potential.

5. Failure strength of silicon carbide containing nanovoids

5.1. Basic concepts about failure strength

Defects such as cracks and voids affect the mechanical behaviour of brittle solids since they modify their overall strength. Often such defects are unavoidable because they form during materials synthesis and processing, but

sometimes they may be introduced by design, in order to obtain specific properties. This is the case of porous materials where pores at a suitable concentration are used to control many properties, like e.g. thermal or acoustic isolation and impact energy absorption. In any case, such inhomogeneities are of great relevance on the mechanical response of the system, since they enhance the local stress and they possibly may initiate failure.

The strength of materials containing cracks and voids is traditionally described according to *stress intensification* or *stress concentration* arguments, respectively [33] The need of different approaches is motivated, according to standard linear elastic fracture mechanics, by the mathematical divergence of the stress field nearby the crack tip: loading a cracked system produces a $1/\sqrt{x}$ singularity at the crack tip (x being the distance from the crack tip along the plane of the crack) and a critical stress equal to zero is expected. As a consequence, a straightforward prediction of failure stress, as uniquely based on local stress criteria, can not be applied. The critical stress of the cracked body is therefore calculated by analyzing the stress singularity at the crack tip: the failure takes place when the stress intensity factor is equal to the material fracture toughness K_c.

Continuum approaches based on stress analysis are based on linear elasticity and they unlikely work at the nanoscale. Their possible weaknesses could in principle be due to the failure of at least one of the three underlying (constitutive) hypotheses they rely on, namely continuum, or elasticity or linearity. In this Section we investigate this issue by addressing the specific problem of a brittle material (crystalline silicon carbide) containing nanovoids, differing by shape and size [34]. We will offer a thorough comparison between atomistic simulations performed as outlined in the previous Sections and we will comment about possible approaches aimed at improving standard continuum models.

5.2. Geometry of the simulation cell and border conditions

The investigated system is defined Fig. 9, where a β-SiC monocrystal - embedding a cylindrical hole - under tensile load σ_A is shown. Similar geometries are adoped for the straight crack and for the spherical hole. In the x-y plane of the simulation cell is kept fixed both in size and shape, and periodically repeated. In this plane the lattice parameter is equal to 4.318 Å. For such a system, as well as for the crack and the spherical hole, we basically want to calculate the failure strength as a function of the defect size and shape, in plane strain border conditions.

In order to generate the differently shaped nanovoids, we follow different procedures. The straigth crack is obtained by cutting a given number of interatomic bonds across a segment of the central plane in the strained simulation cell, which is then relaxed so as to create a Griffith-like hole. We

point out that, because of the very discrete nature of the lattice, there is an arbitrariness - as large as the interbond distance c_0 =2.644 Å along the *x* direction – in defining the actual crack length: this will reflect in the numerical results. The cylindrical and the spherical holes are, in turn, obtained by removing N_h atoms in a selected region of radius *r* at the center of the simulation cell. The actual hole size is defined to be $r + \delta r$, where δr is the maximum variation of the radius that does not modify the number N_h of removed atoms. The cylindrical voids are oriented along the *y* axis, perpendicularly to the applied stress. Finally, in the case of the straight crack, we considered the semilength *r* to vary in the range $c_0 < r < 25c_0$, while the dimension of the cylindrical (spherical) hole ranges within 1.3 Å < *r* < 40 Å (1.3 Å < *r* < 20 Å).

We make use of a simulation cell with dimensions $L_x=L_z=L$ and $L_y \sim 12$ Å for cracks and cylindrical voids, while we select a cubic shape $L_x=L_z=L_y=L$ for spherical holes. In order to avoid finite size effects, we set in any case $L/r>10$. The resulting number of atoms ranges from 3×10^5 to 2.5×10^5 atoms for straight cracks and cylindrical voids, while up to 8×10^5 particles are used for spherical holes.

The atomistic simulations were performed according the dumped dynamics method described in Sec.2 and by adopting the modified Tersoff potential described in the Sec.4. As already commented, the calculated critical strain for β-SiC loaded along the [111] direction are, respectively, $\varepsilon_{zz} \sim 0.20$ and $\sigma_{th}=58$ GPa, in very good agreement with available experimental and ab initio data. Furthermore, the present simulation set-up has proved to be reliable and quantitative in predicting brittle fracture in silicon carbide [35, 36].

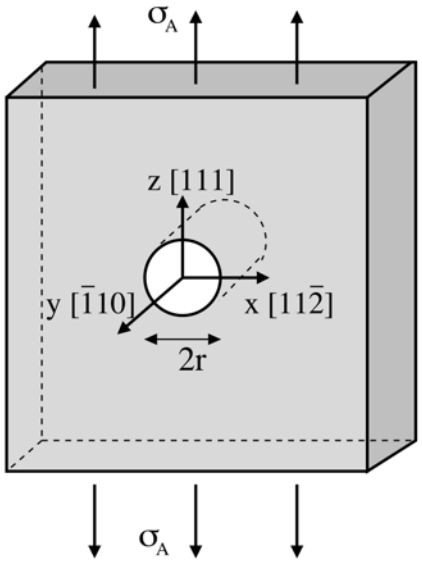

Figure 9. Geometry of a monocrystal containing a cylindrical hole. The system is under strain σ_A applied along the z direction. The alignment of the cartesian axes to the crystallographic directions is reported.

5.3. Results and discussion

The atomistic results for a monocrystal containing a straight crack are reported as full symbols in Fig. 10, as function the crack semilength *r*. At vanishing crack length, the calculated critical stress approaches the theoretical strength σ_{th} of the crystal, as expected. The atomistic results are compared to the standard continuum Griffith theory for brittle fracture (dashed line in Fig. 10): they completely disagree in the region corresponding to a small crack, clearly indicating the need to improve continuum when working at the nanoscale.

In order to improve classical continuum models, modern theories of fracture are generally formulated so as to incorporate into their formalism a suitable material length scale λ [37, 38, 39]: this key quantity is aimed at describing a process zone close to the crack tip where at least one of the standard constitutive hypotheses – namely, continuum, or linearity, or pure elasticity – fails.

The characteristic length scale is typically given by

$$\lambda \approx \frac{2K_c^2}{\pi\sigma_{th}^2} \tag{5.1}$$

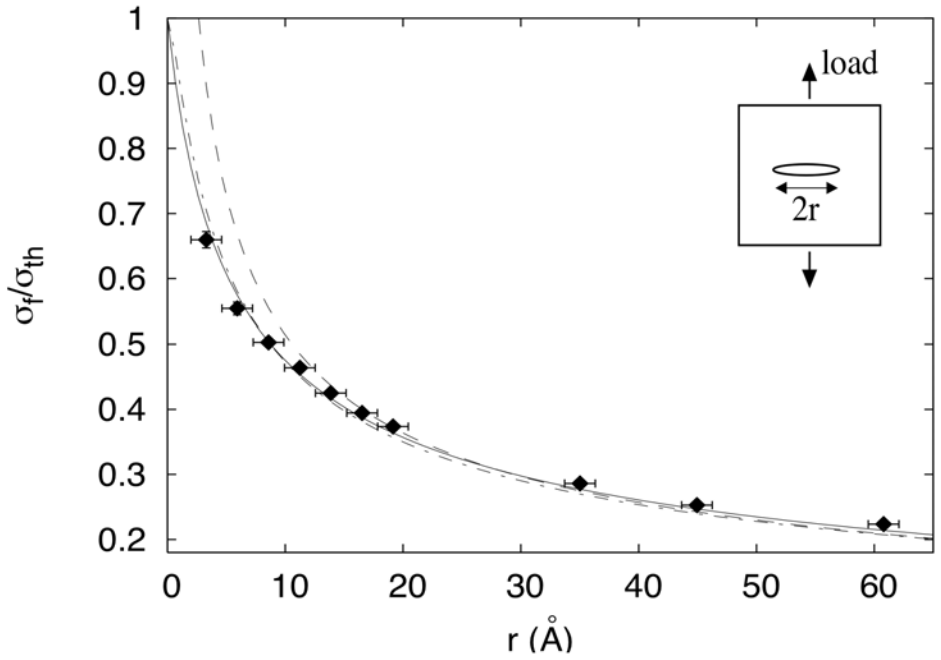

Figure 10. Failure strength of a SiC system containing a crack of semilength r. The loading condition is shown in the inset. Full symbols: atomistic data; dashed line: standard Griffith theory; full and dot-dashed lines: improved continuum models (see text).

The attribution to λ of a physical meaning is not unique and it could be related to the existence of either a plastic zone (i.e. the mechanical response is beyond pure elasticity), or a cohesive zone (linearity is lost) or a discrete unit for crack advancement (continuum hypothesis is no longer applicable). In any case, we point out that none of the above modern theories is able to quantify the actual value of the length scale λ: typically, it must be estimated by fitting from experiments.

Here we have the unique chance to rather use atomistic data as input: this is a much more appealing perspective, since atomistic simulations can be performed under conditions which, by construction, are very close to continuum framework. By using present results as fitting data-base we have determine the actual value of λ (varying in the range 1.4 - 6.0 Å) for two different revised continuum models [34]: the results are shown in Fig. 10 as full and dot-dashed lines, respectively. The agreement is now remarkable and it fully reconciles the atomic-scale picture to continuum one.

The calculated failure strength for a system with an infinite cylindrical hole is represented in Fig. 11 (open diamonds). The observed scattering of the atomistic data depends on the atomic-scale microstructure. A strong dependence of the failure stress σ_f upon the hole size is observed: this is in qualitative contrast to elasticity theory which predicts the costant value σ_f = 1/3 (dotted line). Once again, by revising continuum hypothesis and by indroducing the discrete length scale λ, we can nicely reproduce the atomistic trend of σ_f upon the hole size (full and dot-dashed lines). The fitted lengths are in this case varying in the range 2.2 Å < λ < 6.6 Å: interesting enough, these values differ from the prediction given by eq.(5.1).

Finally, the results for the strength reduction due to a spherical hole are reported in Fig. 12 as full diamonds. Even in this case, atomistic simulations prove that σ_f strongly depends upon the hole size, while standard elasticity predicts the costant value σ_f = 1/2 (dashed line). The best fits with improved continuum models are shown by full and dot-dashed lines and are obtained by setting 2.8 Å < λ < 7.9 Å. Once again these values are quite different than the estimations provided by eq.(5.1).

In conclusions, the present results seem to indicate that a continuum formalism enclosing the concept of a relevant length scale (or process zone) for failure strength works definitely better than standard elasticity. However, eq.(5.1) must be considered as a tool for estimating just the order of magnitude of such a process zone, since its actual value can only be quantitatively estimated by means of a fully atomistic approach. Present simulations further prove that λ is not a physical material parameter; rather, it is related to the system geometry. In particular, it is found that the process zone is larger for holes than for cracks.

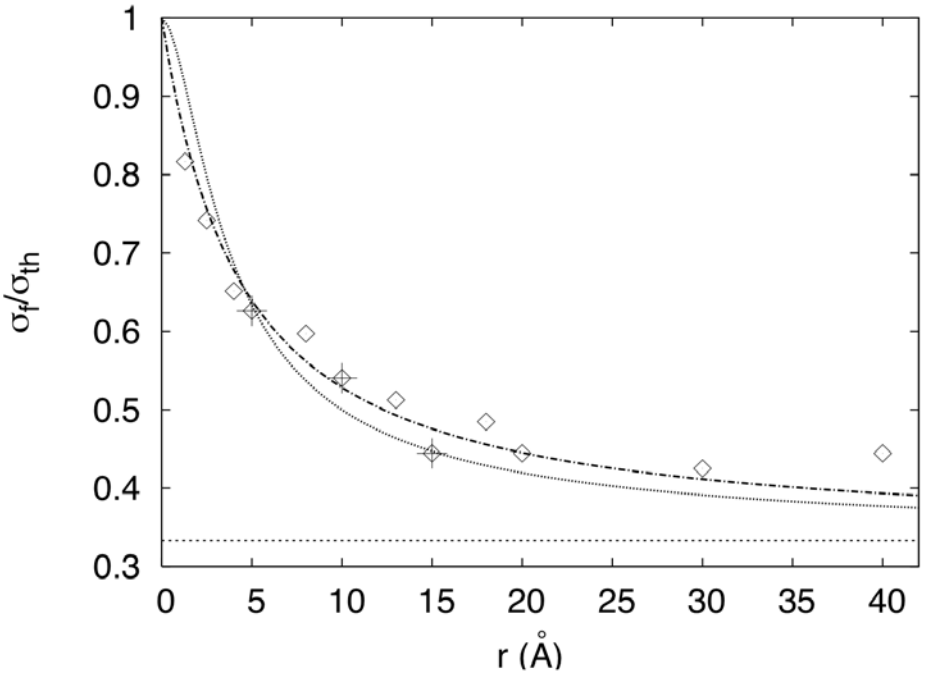

Figure 11. Failure strength of a system containing a cylindrical hole of radius r. Open diamonds: atomistic data; dotted line: linear elastic theory; full and dot-dashed lines: improved continuum models (see text).

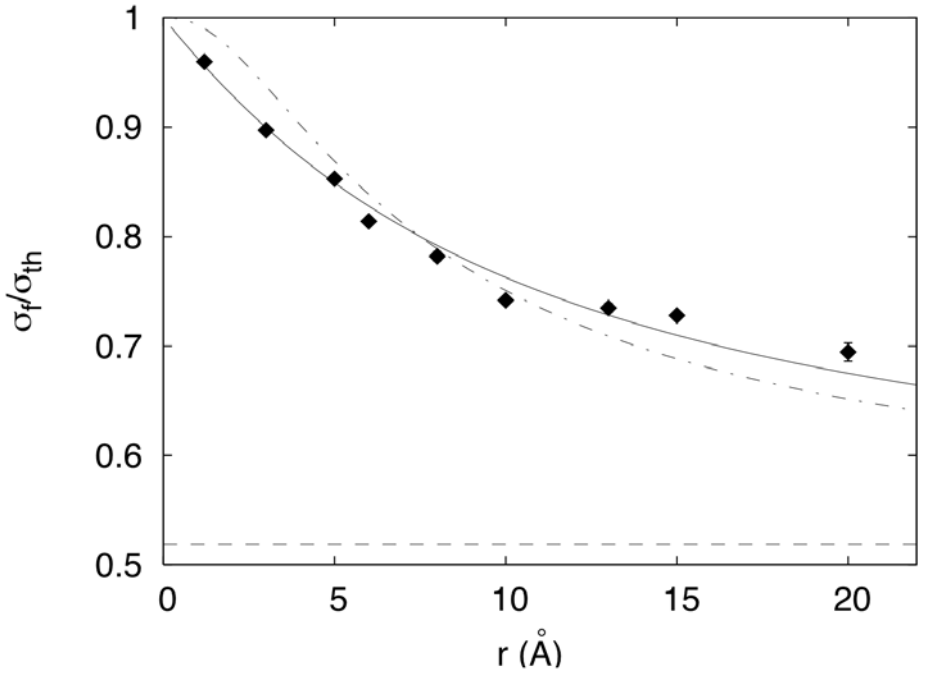

Figure 12. Failure strength of a system containing a sphericall hole of radius r. Full diamonds: atomistic data; dashed line: linear elastic theory; full and dot-dashed lines: improved continuum models (see text).

Acknowledgements

This work makes use of results produced by the Cybersar Project managed by the Consorzio COSMOLAB, a project co-funded by the Italian Ministry of University and Research (MUR) within the Programma Operativo Nazionale 2000-2006 "Ricerca Scientifica, Sviluppo Tecnologico, Alta Formazione" per le Regioni Italiane dell'Obiettivo 1 (Campania, Calabria, Puglia, Basilicata, Sicilia, Sardegna) – Asse II, Misura II.2 "Società dell'Informazione", Azione a " Sistemi di calcolo e simulazione ad alte prestazioni".

More information is available at http://www.cybersar.it

References

1. L. Xiantao and E. Weinan 2005 J. Mech. Phys. Solids **53** 1650.
2. J.D. Clayton and P.W. Chung 2006 J. Mech. Phys. Solids **54** 1604.
3. D. Marx, J. Hutter NIC and F.Z. Jülich 2000 *Ab Initio Molecular Dynamics: Theory and Implementation*, in *Modern Methods and Algorithms of Quantum Chemistry* edited by J. Grotendorst.
4. M. P. Allen and D. J. Tildesley 1991 *Computer simulation of liquids* (Clarendon Press, Oxford).
5. D. Frenkel and B. Smit 1996 *Understanding molecular simulations* (Academic Press, San Diego.
6. M. Finnis 2003 *Interatomic forces in condesed matter* (Oxford University Press, Oxford).
7. M. Ippolito, G. Fugallo, A. Mattoni, L. Colombo and F. Cleri 2005 Strength, Fracture and Complexity **3** 89.
8. F. Cleri 2002 Phys. Rev. B **65** 014107.
9. A. J. Fresnel 1868 *Oeuvres Complètes*, Imprimerie Impériale, Paris, pp. 343-367.
10. C. L. M. H. Navier 1822 *Mémoire sur les lois de l'équilibre et du mouvement des corps solides élastiques* Mémoires de l'Académie des Sciences de l'Institut de France vol 7 pp. 375-393.
11. A. L. Cauchy 1823 *Recherches sur l'équilibre et le mouvement intérieur des corps solides ou fluides, élastiques ou non élastiques* Bulletin de la Société Philomathique pp. 9-13.
12. A. L. Cauchy 1827 *Sur les relations qui existent dans l'état d'équilibre d'un corps solide ou fluide, entre les pressions ou tensions et les forces accélératrices* Exercices de Mathématique vol. 2 pp. 108-111.
13. W. Voigt 1887 *Theoretische Studien über die Elasticitätsverhaltnisse der Krystalle* Abhandlungen der königlichen Gesellschaft der Wissenschaften zu Göttingen vol.34.
14. D. Capecchi, G. Ruta and R. Tazzioli 2006 *Enrico Betti: teoria della elasticità* Hevelius Edizioni Benevento.
15. I. Todhunter 1893 *A History of the Theory of Elasticity and of the Strength of Materials from Galilei to the Present Time* Cambridge University Press.
16. L. D. Landau and E. M. Lifschitz 1959 *Theory of Elasticity* (Pergamon Press, New York).
17. D. Hollad and M. Marder 1999 Adv. Mater **11**, 783.

18. M. Tang and S. Yip 1995 Phys. Rev. B **52** 15150.
19. D. Holland and M. Marder 1998 Phys. Rev. Lett. **80** 746.
20. N. Bernstein and D. W. Hess 2003 Phys. Rev. Lett. **91** 025501.
21. H. Kicuchi, R. K. Kalia, A. Nakano, P. Vashista, P. Branicio and F. Shimojo 2005 J. Appl. Phys. **98** 103524.
22. J. G. Swadener, M. I. Baskes and M. Nastasi 2002 Phys. Rev. Lett. **89** 085503.
23. J. H. Rose, J. R. Smith, F. Guinea and J. Ferrante 1984 Phys. Rev. B **29** 2963.
24. R. Perez and P. Gumbsch 2000 Phys. Rev. Lett. **84** 5347.
25. P. Gumbsch (editor) 2006 *Conference Proceedings, 3rd Int. Conference Multiscale Materiasl Modeling*, Frunhofer-Istitute for Mechanics of Materials, Freiburg.
26. G. Lu and E. B. Tadmor and E. Kaxiras 2006 Phys. Rev. B **73** 024108.
27. C. Csanyi, T. Albaret, M. C. Payne and De Vita 2004 Phys. Rev. Lett. **93** 175503.
28. M. J. Buehler, A. C. T. van Duin and W. A. Goddard III 2006 Phys. Rev. Lett. **96** 095505.
29. W. R. L. Lambrecht, B. Segall, M. Methfessel and M. van Schilfgaarde 1991 Phys. Rev. B **44** 3685.
30. A. Mattoni, M. Ippolito and L. Colombo 2007 submitted for publication.
31. J. Tersoff 1989 Phys. Rev. B **39** 5566.
32. W. Li and T. Wang 1999 Phys. Rev. B **59**, 3993.
33. K.B. Broberg Academic, San Diego, 1999 *Cracks and Fracture*.
34. M. Ippolito, A. Mattoni, N. Pugno, and L. Colombo 2007 Phys. Rev. B **75** 224110.
35. A. Mattoni, L. Colombo, and F. Cleri 2005 Phys. Rev. Lett. **95** 115501.
36. M. Ippolito, A. Mattoni, L. Colombo, and F. Cleri 2005 Appl. Phys. Lett. **87** 141912.
37. J.M. Whitney and R.J. Nuismer 1974 J. Compos. Mater. **8** 253.
38. R.J. Nuismer and J.M. Whitney 1975 ASTM Spec. Tech. Publ. **553** 117.
39. N.M. Pugno and R.S. Ruoff 2004 Philos. Mag. **84** 2829.